Letter

Experimental demonstration of a quantum engine driven by entanglement and local measurements

Kunkun Wang,[1,2] Ruqiao Xia,[1,3] Léa Bresque,[4] and Peng Xue[1,*]

[1]*Beijing Computational Science Research Center, Beijing 100084, China*
[2]*School of Physics and Optoelectronic Engineering, Anhui University, Hefei 230601, China*
[3]*Cavendish Laboratory, University of Cambridge, Cambridge CB3 0HE, United Kingdom*
[4]*Université Grenoble Alpes, CNRS, Grenoble INP, Institut Néel, 38000 Grenoble, France*

(Received 30 April 2022; accepted 12 September 2022; published 22 September 2022)

Understanding entanglement and quantum measurements from a thermodynamics point of view is a fundamental and challenging task. Recently, a two-qubit engine was put forward as an appropriate platform to tackle these challenges. Here we achieve an experimental simulation and provide the direct experimental proof of these findings using single photons and linear optics. Encoding the qubits by polarization and transverse spatial modes of single photons, entanglement is created through the interaction between them. We show that, upon local measurement, classical mutual information can be extracted in order to fuel a quantum measurement engine. By measuring the energy changes, we identify that the energy gain comes from the measurement channel and corresponds to the cost of erasing the quantum correlations between qubits. The scheme is further generalized to an N-qubit chain for energy upconversion. Our experimental results provide a thorough understanding of this quantum engine with entanglement and local measurements as a new kind of fuel, as well as a general platform for exploration of quantum engines.

DOI: 10.1103/PhysRevResearch.4.L032042

I. INTRODUCTION

A usual task of an engine is to extract mechanical work from a hot bath in a cyclically repeated way [1–3]. Although the goal is the same, the source of stochasticity can be different when the working substance of the engine is quantum. Analysis of the quantum engine was first introduced by Scovil and Schulz-Dubois [4], where three-level masers were used as the working substances for heat engines. Since then, many efforts have been devoted to studying quantum effects in thermodynamic [5,6] and quantum analogs of the classical engines [7–12]. Enthusiastic interest in quantum engines is growing with possibilities of overcoming the traditional classical efficiency limit [12,13], better understanding of thermalization in the quantum realm [14,15], and controlling nonequilibrium dynamics of microscopic systems [16–18].

To understand the impact quantum thermodynamic effects can have, the role of quantum measurements especially attracts attention. Both selective measurements [19–23] (or the read measurements with projecting the measured systems to the selected eigenstate) and nonselective measurements [24–26] (or unread measurements, the averaging of a selective one over all the possible outcomes) have been used as a kind of fuel in so-called measurement-driven engines. However, in these previous studies [27–30], classical measuring devices have been used and the fuel is identified with the energetic counterpart of the measurement postulate. Recently, a quantum engine powered by entanglement and local measurements was designed by Bresque *et al.* [31], in which quantum measurements collapse the engine in some specific states that may change the energy of the engine. Thus, similar to a bath, measurements behave as a source of entropy and energy.

In this work, we experimentally simulate a quantum measurement powered engine made of two qubits encoded by two different degrees of freedom of single photons, which become entangled through coherence exchange of a quantum excitation realized by an interferometric network. We implement the local measurement, which is modeled as the entanglement between a qubit and a meter, and then identify the fuel as the energetic cost to erase quantum correlation. By applying the feedback according to the information extracted by the measurement, the results show that the work efficiency increases with the information extracted from the measurement. All these processes, including evolution of interaction between two qubits, local measurements, and feedback, are realized with single photons and linear optics. Furthermore, we extend the scheme to an N-qubit engine experimentally. Our experimental results provide a deeper understanding of entanglement and local measurements as fuels in quantum engines.

II. EXPERIMENTAL DEMONSTRATION

We experimentally realize a quantum engine consisting of two qubits A and B with transition frequencies ω_A and ω_B ($\omega_A < \omega_B$, $\delta = \omega_B - \omega_A$), respectively, which are governed by

[*]gnep.eux@gmail.com

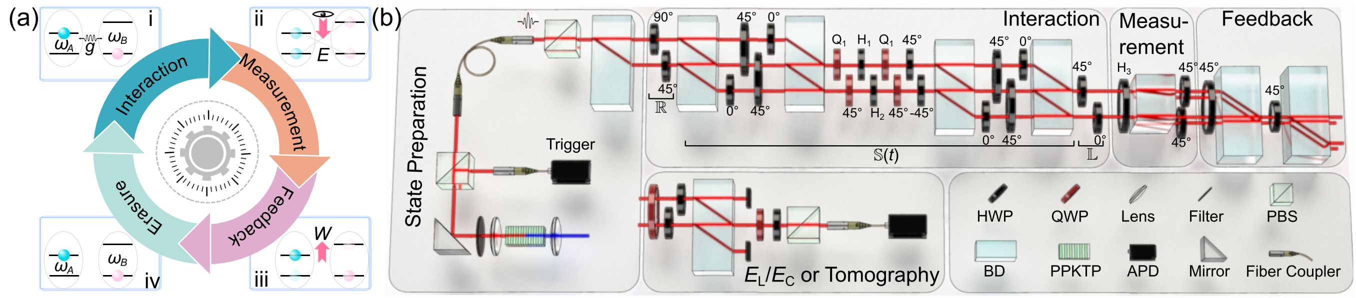

FIG. 1. (a) Illustration of a two-qubit engine cycle: (i) entangling evolution, (ii) measurement, (iii) feedback, and (iv) erasure. (b) Experimental setup. A photon pair is generated by the spontaneous parametric downconversion in the periodically polled potassium titanyl phosphate crystal (PPKTP), with one serving as the trigger and the other injected into the interferometric network as a heralded single photon. The initial state of the two qubits is prepared in $|RH\rangle$. Subsequently, a unitary operation $U(t)$ is realized by an interferometric network consisting of beam displacers (BDs), half-wave plates (HWPs), and quarter-wave plates (QWPs). To realize the local measurement on B, another BD is applied to extend the spatial modes, which are used to encode the meter qubit. The feedback is realized by two BDs and the HWPs placed in different spatial modes due to the outcomes of the measurement on B. Projective measurements and state tomography are used to measure the energy and entropy of the engine, respectively. Photons are detected by coincidence using silicon avalanche photodiodes (APDs).

a Hamiltonian [31],

$$H_{\mathrm{T}} = H_{\mathrm{L}} + H_{\mathrm{C}}. \tag{1}$$

Here $H_{\mathrm{L}} = \sum_{i=A,B} \hbar\omega_i \xi_i^\dagger \xi_i$ ($\xi_i = |0\rangle_i\langle 1|$) and $H_{\mathrm{C}} = \hbar g(\xi_A^\dagger \xi_B + \xi_B^\dagger \xi_A)/2$ are the free and interaction Hamiltonians, respectively, and g is the coupling strength. For convenience, we choose $\hbar = 1$ in the following. In our experiment, qubit A is encoded in the left and right transverse spatial modes of single photons generated via spontaneous parametric downconversion, i.e., $|0\rangle \Leftrightarrow |L\rangle$ and $|1\rangle \Leftrightarrow |R\rangle$, whereas B is encoded in their horizontal and vertical polarizations, i.e., $|0\rangle \Leftrightarrow |H\rangle$ and $|1\rangle \Leftrightarrow |V\rangle$.

As illustrated in Fig. 1(a), there are four strokes for an engine cycle: (i) entangling evolution, (ii) measurement, (iii) feedback, and (iv) erasure. The first three are realized by the setup in Fig. 1(b).

In the first stroke, qubit A is initially prepared in an excited state and B in a ground state, i.e., $|\psi(0)\rangle_{AB} = |10\rangle = |RH\rangle$. The initial state is generated by single photons passing through a polarizing beam splitter (PBS) and a beam displacer (BD). The initial energy of the working substance is $E_{\mathrm{T}}(0) = E_{\mathrm{L}}(0) + E_{\mathrm{C}}(0) = \mathrm{Tr}[|\psi(0)\rangle\langle\psi(0)|H_{\mathrm{T}}] = \omega_A$, where $E_{\mathrm{L}}(0) = \omega_A$ and $E_{\mathrm{C}}(0) = 0$ are the local and binding energies, respectively. As the engine is thermally isolated, the evolution with the total interaction time τ can be described by a unitary operator $U(\tau) = e^{-\frac{i}{\hbar}H_{\mathrm{T}}\tau}$, which can be decomposed as $U(\tau) = \mathbb{L}\mathbb{S}(\tau)\mathbb{R}$ (see Appendix A for details). The controlled operators $\mathbb{L}$ and $\mathbb{R}$ can be realized by inserting half-wave plates (HWPs) in the corresponding spatial modes serving as the control qubit, while $\{|H\rangle, |V\rangle\}$ is the target qubit. For $\mathbb{S}(\tau)$, the polarization of photons serves as the control qubit and the spatial mode is the target qubit. Then, $\mathbb{S}(\tau)$ can be implemented by a cascaded interferometric network consisting of BDs, HWPs, and quarter-wave plates (QWPs) with certain setting angles $H_1 = (2\theta - \Omega\tau - \pi)/4$, $H_2 = (\pi - \omega_A\tau - \omega_B\tau)/4$, and $Q_1 = (2\theta - \pi)/4$ [32]. Here $\Omega = \sqrt{g^2 + \delta^2}$ is the Rabi frequency characterizing the periodic excitation exchange with period $2\pi/\Omega$ and $\tan\theta = g/\delta$. Thus, for entangling evolution, the detuning δ, the coupling strength g, and the total interaction time τ can be varied by tuning the angles of wave plates (H_1, H_2, Q_1) accordingly. After this stroke, the qubits get entangled. Energy evolution is characterized by achieving projective measurements with a BD and wave plates.

In the second stroke, the engine is instantly coupled to a classical measuring device, which performs a projective measurement on qubit B at time τ instantaneously. We simulate this process by involving a third qubit as the meter to store the measured outcome. Another two longitudinal spatial modes of photons are introduced to encode the meter qubit, i.e, $|0\rangle \Leftrightarrow |U\rangle$ and $|1\rangle \Leftrightarrow |D\rangle$. The initial state of the meter is $|U\rangle$. The measurement is captured by a controlled unitary operator $U_M = \mathbb{1}_A \otimes (|H\rangle_B\langle H| \otimes \mathbb{1}_M + |V\rangle_B\langle V| \otimes X_M)$, which flips the state of the meter if qubit B is in the excited state $|V\rangle$, and does nothing otherwise. Here $\mathbb{1}_i$ ($i = A$ or M) is the identity operator and $X_M = |U\rangle_M\langle D| + |D\rangle_M\langle U|$ is the flipping operator. The unitary operator U_M on the polarizations and longitudinal spatial modes of photons is realized by HWPs and a BD whose optical axis is perpendicular to that of the one used in the first stroke.

By setting $\tau = \pi/\Omega$ and tracing out the meter, the state of the effective two-qubit system becomes a mixed state $\rho_{AB} = \cos^2\theta|RH\rangle\langle RH| + \sin^2\theta|LV\rangle\langle LV|$. Quantum correlations between the two qubits are then erased, implying that the binding energy E_{C} would tend to zero. The mean energy $E_{\mathrm{meas}} = -E_{\mathrm{C}}(\tau = \frac{\pi}{\Omega}) = \delta\sin^2\theta$ gained from the measurement thus corresponds to the cost to erase the quantum correlations. The local measurement also increases the von Neumann entropy of the engine $S_{\mathrm{meas}} = -\mathrm{Tr}[\rho_{AB}\log_2\rho_{AB}] = -\cos^2\theta\log_2(\cos^2\theta) - \sin^2\theta\log_2(\sin^2\theta)$.

Note that the fueling step only involves the characteristics of the qubits, which does not fully describe the measurement process as it also creates classical correlations between the qubits and the meter. The classical correlation is quantified by the classical mutual information $I(AB:M) = H(\rho_{AB}) + H(\rho_M) - H(\rho_{ABM})$, where $H(\rho) = \sum_i -p_i\log_2 p_i$ is the Shannon entropy and p_i is the probability of the state ρ being found in $|i\rangle$. For an ideal measurement, $I(AB:M) =$

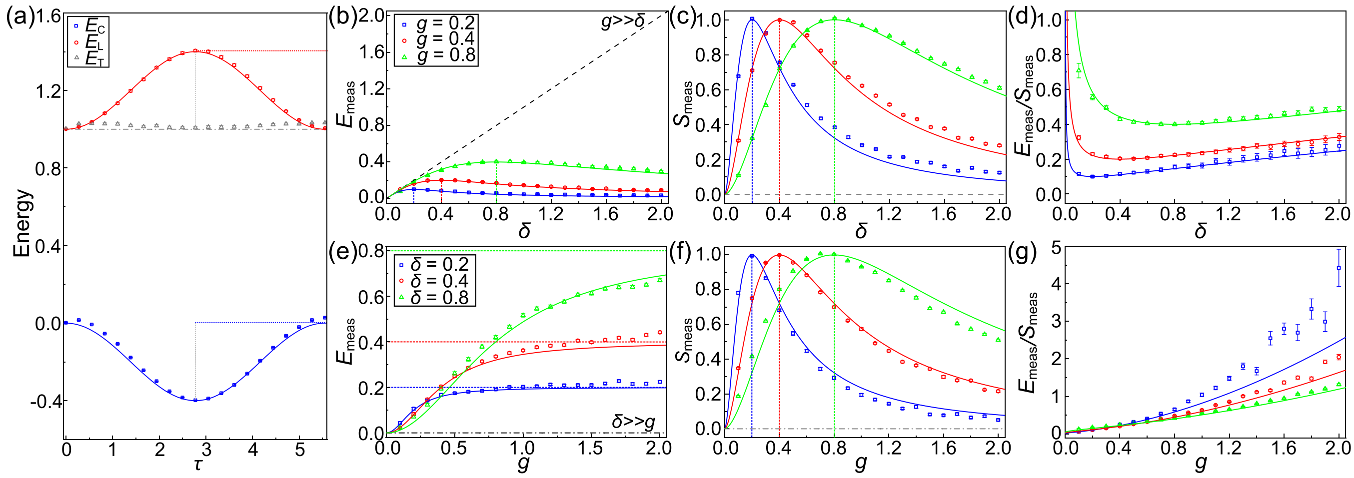

FIG. 2. (a) Evolution of the local energy E_{L} (red solid line), binding energy E_{C} (blue solid line), and total energy E_{T} (gray dashed line) as a function of τ with fixed $\omega_A = 1$ and $\delta = g = 0.8$. (b) The mean energy E_{meas} and (c) entropy S_{meas} input by the measurement process and their ratio $E_{\mathrm{meas}}/S_{\mathrm{meas}}$ as a function of the detuning δ with various coupling strength g and fixed $\omega_A = 1$. The black dashed lines indicate the limit $g \gg \delta$. (e) E_{meas}, (f) S_{meas}, and (g) $E_{\mathrm{meas}}/S_{\mathrm{meas}}$ as a function of g with various δ and fixed $\omega_A = 1$. The black dot-dashed lines indicate the limit $\delta \gg g$. Experimental data are represented by color symbols. Error bars are due to the statistical uncertainty in photon-number counting.

S_{meas} is satisfied. For an imperfect measurement with an error probability P of the meter being found in $|D\rangle$ ($|U\rangle$) and the qubit B in $|H\rangle$ ($|V\rangle$), the extracted classical mutual information is less, i.e., $I(AB:M) < S_{\mathrm{meas}}$. By varying the angles of the HWP in front of the BD, $H_3 = \arcsin\sqrt{P}/2$, we can realize measurements with various error probabilities $P \in [0, 0.5]$. For $P = 0$, the ideal measurement is implemented. For $P = 0.5$, the imperfect measurement cannot yield any information.

In the stroke of feedback, the information stored in the meter is now processed to convert the fuel into work. If the excitation is measured in B, a bit flip operation is performed on both A and B. If the excitation is measured in A, nothing is done. We achieve this stroke by a controlled unitary operation of $U_F = \mathbb{1}_{AB} \otimes |U\rangle_M\langle U| + X_{AB} \otimes |D\rangle_M\langle D|$, where $\mathbb{1}_{AB}$ (X_{AB}) is the identity (flipping) operator. Therefore, the work extraction process is simulated and then the qubits are reset to their initial states. The controlled operation U_F can be realized via two BDs and two HWPs at 45° placed in different longitudinal spatial modes due to the outcomes of the measurement on B.

If all information is consumed, i.e., $W = E_{\mathrm{meas}}$, the conversion is optimal. After this stroke, the qubits' entropy vanishes and the classical mutual information is consumed completely, whereas an incomplete consumption of information yields a conversion ratio $\eta = W/E_{\mathrm{meas}} < 1$. To quantify the energy and entropy of the engine, projective measurements and state tomography are realized with a BD and wave plates [33]. The probability p_i in the classical mutual information $I(AB:M)$ is measured by projecting the state to the computational basis of both the qubits and the meter. The extracted work can be quantified by the changes of the energy before and after the stroke of feedback.

Finally, the correlation between the meter and the engine is erased and the working substances combined with the meter are initialized for the next cycle of the engine [34].

III. EXPERIMENTAL RESULTS

The evolution of the local and binding energies in a period of the interaction with fixed $\omega_A = 1$ and $\delta = g = 0.8$ is shown in Fig. 2(a). The periodic exchange of the single excitation between two qubits gives rise to oscillations (opposite oscillations) of the local energy (binding energy). The sum of the energies remains constant and equals the energy of the initial state theoretically. Our experimental results agree well with the theoretical predictions [31]. The small experimental discrepancies from theory are caused by several factors, including fluctuations in photon numbers, the inaccuracy of wave plates, and dephasing due to the misalignment of the BDs.

The mean energy E_{meas} and entropy S_{meas} input by the measurement process and their ratio $E_{\mathrm{meas}}/S_{\mathrm{meas}}$ as a function of the detuning δ with various g and fixed $\omega_A = 1$ are shown in Figs. 2(b)–2(d), whereas those as a function of g with various δ and fixed $\omega_A = 1$ are shown in Figs. 2(e)–2(g). The entropy S_{meas} is maximized for $\delta = g$. The mean energy E_{meas} increases with g and approaches the maximized values for $g \gg \delta$. For $\delta \gg g$, E_{meas} is always zero, which implies that local measurements and entanglement cannot be used as fuels in this situation. For either of the limits $g \gg \delta$ and $\delta \gg g$, S_{meas} is always zero. The ratio of $E_{\mathrm{meas}}/S_{\mathrm{meas}}$ characterizes the efficiency of information-to-work conversion. Compared to the engine fueled by a thermal bath [35,36], in which such efficiency is bounded by the bath temperature, the efficiency in Fig. 2(g) is not bounded and increases as g. In the limit $g \gg \delta$, a finite amount of work can be extracted with vanishing a small amount of entropy.

The work extraction ratio η as a function of the detuning δ and the classical mutual information $I(AB:M)$ with fixed $\omega_A = 1$ and $g = 0.8$ is shown in Fig. 3(a), which clearly indicates that the larger work value of information corresponds to the larger conversion ratio. Figures 3(b) and 3(c) feature

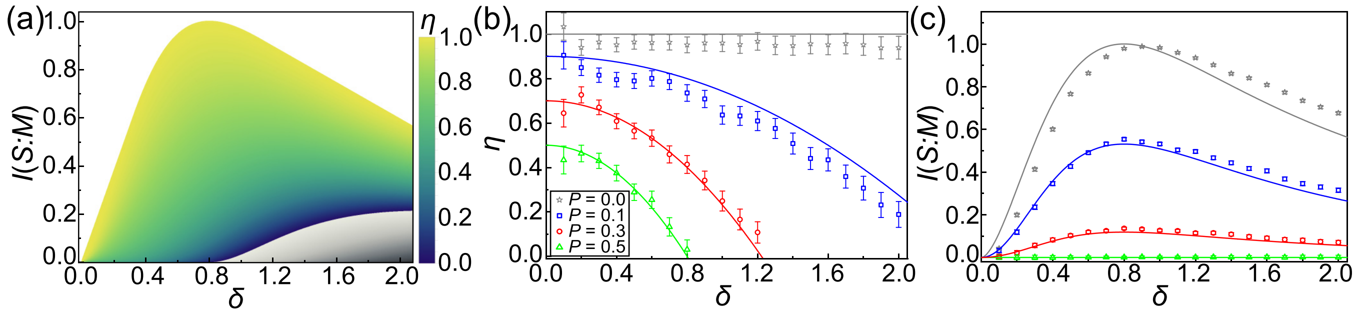

FIG. 3. (a) Theoretical predictions of the work extraction ratio η (color scale) as a function of the detuning δ and the classical mutual information $I(AB : M)$. The parameters $\omega_A = 1$ and $g = 0.8$ are fixed. The gray area corresponds to $\eta \leqslant 0$, where energy cannot be extracted during feedback. Experimental results of (b) η and (c) $I(AB : M)$ as a function of δ with various error probabilities P. Theoretical predictions are shown in colored curves and experimental data are represented by color symbols. Error bars are due to the statistical uncertainty in photon-number counting.

the work extraction ratio and the classical mutual information as a function of δ with various error probabilities P, which indicates that the larger the error probability P, the lower the ratio η and the smaller the classical mutual information. For an imperfect cycle with $P > 0$, the ratio decreases with increasing δ. Interestingly, for $\delta < g$, the work can be extracted even if $P = 0.5$ and the classical mutual information $I(AB : M)$ equals zero.

IV. GENERALIZATION TO N QUBITS

As depicted in Fig. 4(a), the fueling mechanism can be extended to an N-qubit chain with increasing frequencies [31]. The frequency of qubit i is $\omega_i = \omega_A + (i-1)\delta/(N-1)$, where $i = 1, \dots, N$; $\omega_1 = \omega_A$; and $\omega_N = \omega_B$, that is, the detuning between every two adjacent qubits by $\delta/(N-1)$. Driven by entanglement and local measurements, the low energy of the first qubit A can be upconverted to an arbitrarily high energy at the last qubit B. At time $t = 0$, the first qubit A is in the excited state and the coupling between A and the second qubit is turned on with the Rabi frequency $\Omega_N = \sqrt{g^2 + \delta^2/(N-1)^2}$ and the coupling coefficient g. At time $t = \pi/\Omega_N$, a local measurement is performed on the second qubit. If the excitation is found, the same process is applied in the second and third qubits. Repeating the same tasks constantly, qubit B will be detected in the excited state with probability $P_{\text{succ}} = \sin^{2(N-1)}\theta_N$, where $\tan\theta_N = (N-1)g/\delta$.

Energy upconversion can be simulated by translating the measurements on different qubits in the chain to those on two qubits at different times [37], in which the entangling evolution of each adjacent two qubits can be realized by two BDs and wave plates (see Appendix B for details). The local measurement on the qubit can be realized by ruling out photons with one of the spatial modes $|R\rangle$ and passing photons in $|L\rangle$ through for further evolution. After $N-1$ times interaction and measurement, the successful probability of energy upconversion is the probability of the final state being found in $|LV\rangle$.

Figure 4(b) shows the measured successful probability P_{succ} of energy upconversion as a function of g with fixed $\omega_A = 1$ and $\delta = 0.8$. By setting $N = 2$, $N = 4$, and $N = 6$, the experimental results suggest that P_{succ} increases with both the coupling strength g and the length of the chain N. For the limit $g \to \infty, N \to \infty$, the last qubit B is found in the excited state deterministically.

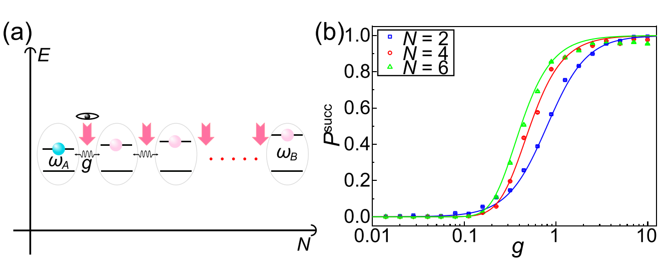

FIG. 4. (a) Entanglement and local measurements based energy upconversion by extending the fueling mechanism to a chain of N qubits. (b) Measured successful probability P_{succ} of energy upconversion as a function of g with various chain length N, fixed $\omega_A = 1$, and $\delta = 0.8$. Theoretical predictions are shown in colored curves and experimental data are represented by color symbols. Error bars are due to the statistical uncertainty in photon-number counting.

V. CONCLUSION

We report the experimental simulation of a two-qubit engine fueled by entanglement and local measurements. We implement a cycle of this engine at the quantum level with single photons and provide a typical and successful exploration of the entanglement engines fueled by quantum measurements. Experimental results explicitly show that the engine efficiency can approach unity by fully consuming the information carried by measurement. Compared to the Szilard engine [38,39], in our experiment, the work can be extracted without any information about qubits. We also show that the two-qubit engine can be extended to multiqubit ones by extending the spatial modes of single photons. Thus, the experimental work provides a versatile platform for the systematic experimental study of quantum engines and will inspire further investigation of entanglement quantum engines in various physical platforms [40–42]. Our studies shed light on the fueling mechanism and will contribute to future engines starting to use quantum measurements as fuels.

ACKNOWLEDGMENTS

We thank Prof. Alexia Auffèves for helpful discussions. This work has been supported by the National Natural Science Foundation of China (Grants No. 12025401, No. 12104009, No. U1930402, and No. 12088101).

APPENDIX A: FURTHER INFORMATION FOR EXPERIMENTAL IMPLEMENTATION

A pair of photons is created via spontaneous parametric downconversion, one serving as a trigger and the other as a heralded single photon. Qubit A is encoded in the left and right transverse spatial modes of the photon, i.e., $|0\rangle \Leftrightarrow |L\rangle$ and $|1\rangle \Leftrightarrow |R\rangle$, whereas qubit B is encoded in the horizontal and vertical polarization degrees of the photon, i.e., $|0\rangle \Leftrightarrow |H\rangle$ and $|1\rangle \Leftrightarrow |V\rangle$. After the single photons pass through a PBS and a BD, the initial state of the two qubits is then in $|RH\rangle$.

For interaction, the unitary operator can be decomposed as $U(\tau) = \mathbb{L}\mathbb{S}(\tau)\mathbb{R}$, where $\mathbb{L}$, $\mathbb{S}(t)$, and $\mathbb{R}$ are the controlled two-qubit gates [32]. For $\mathbb{R}$ and $\mathbb{L}$, the spatial mode of photons serves as the control qubit and the polarization mode is the target qubit, i.e.,

$$\mathbb{R} = |L\rangle\langle L| \otimes (-|H\rangle\langle H| + |V\rangle\langle V|) + |R\rangle\langle R| \otimes (|H\rangle\langle V| + |V\rangle\langle H|), \tag{A1}$$

$$\mathbb{L} = |L\rangle\langle L| \otimes (|H\rangle\langle V| + |V\rangle\langle H|) + |R\rangle\langle R| \otimes (|H\rangle\langle H| - |V\rangle\langle V|). \tag{A2}$$

As shown in Fig. 2 of the main text, $\mathbb{R}$ is realized by inserting HWPs at 90° and 45° in the left and right spatial modes, respectively. Similarly, $\mathbb{L}$ is realized by inserting HWPs at 45° and 0° in the left and right spatial modes. For $\mathbb{S}(\tau)$, the polarization of photons is the control qubit and the spatial mode is the target one. Thus, it can be further decomposed as $\mathbb{S}(\tau) = \mathbb{T}\mathbb{M}(\tau)\mathbb{T}$, where

$$\mathbb{T} = \begin{pmatrix} 0 & 1 & 0 & 0 \\ 0 & 0 & 0 & 1 \\ 1 & 0 & 0 & 0 \\ 0 & 0 & 1 & 0 \end{pmatrix} \tag{A3}$$

is realized by using a set of HWPs at 45° and 0° and two BDs, and

$$\mathbb{M}(\tau) = |L\rangle\langle L| \otimes U_L(t) + |R\rangle\langle R| \otimes U_R(\tau) \tag{A4}$$

is realized by inserting wave plates in the certain spatial mode. Here U_L and U_R are unitary operations acting on the polarization mode, i.e.,

$$U_L = \begin{pmatrix} -i\sin\theta\sin\frac{t\Omega}{2} & \cos\frac{t\Omega}{2} + i\cos\theta\sin\frac{t\Omega}{2} \\ \cos\frac{t\Omega}{2} - i\cos\theta\sin\frac{t\Omega}{2} & -i\sin\theta\sin\frac{t\Omega}{2} \end{pmatrix},$$
$$U_R = \begin{pmatrix} 0 & -e^{-\frac{it(\omega_A+\omega_B)}{2}} \\ -e^{\frac{it(\omega_A+\omega_B)}{2}} & 0 \end{pmatrix}. \tag{A5}$$

This method [32] can be used to decompose any higher dimensional unitary operations.

Setting $\tau = \pi/\Omega$, the state of engine is evolved to $|\psi_{AB}(\tau = \pi/\Omega)\rangle = i(\cos\theta|RH\rangle - \sin\theta|LV\rangle)$. At this time, a local measurement is instantaneously performed on qubit B and its outcome is encoded in a meter M. In our experiment, another two longitudinal spatial modes of photons are introduced to encode the meter qubit, i.e, $|0\rangle \Leftrightarrow |U\rangle$ and $|1\rangle \Leftrightarrow |D\rangle$. The initial state of the meter is $|U\rangle$. The local measurement with various error probabilities $P \in [0, 0.5]$ on B is achieved by three HWPs and a BD whose optical axis is perpendicular to that of the one used in the first stroke. The angle of the HWP in front of the BD is set to $H_3 = \arcsin\sqrt{P}/2$ and two HWPs right behind the BD are set to 45°. Subsequently, the state of the engine combined with the meter after the measurement is

$$|\psi_{ABM}\rangle = i\cos\theta|RH\rangle(\sqrt{1-P}|U\rangle + \sqrt{P}|D\rangle) - i\sin\theta|LV\rangle(\sqrt{P}|U\rangle + \sqrt{1-P}|D\rangle). \tag{A6}$$

To quantify the total energy during different strokes, the system is projectively measured in such a way as to obtain the average of its total energy compose of the local and binding contribution. With $H_{\rm L} = \omega_B|LV\rangle\langle LV| + \omega_A|RH\rangle\langle RH| + (\omega_A + \omega_B)|RV\rangle\langle RV|$ and $H_{\rm C} = \sum_{\pm} g/4(|LV\rangle \pm |RH\rangle)(\langle LV| \pm \langle RH|)$, we achieve the projective measurements in the basis of $\{|LH\rangle, |LV\rangle, |RH\rangle, |RV\rangle, (|LV\rangle+|RH\rangle)/2, (|LV\rangle-|RH\rangle)/2\}$ by using a BD, two QWPs, three HWPs, and a PBS. The mean energy $E_{\rm meas}$ can thus be obtained by measuring the total energy difference between before and after the stroke of measurement, and the extracted work W is obtained by measuring the total energy difference between before and after the stroke of feedback. For the increased von Neumann entropy $S_{\rm meas} = -{\rm Tr}[\rho_{AB}\log_2\rho_{AB}]$, it can be obtained by constructing ρ_{AB} via state tomography, where 16 measurements in the bases of $\{|L\rangle, |R\rangle, (|L\rangle - i|R\rangle)/2, (|L\rangle + |R\rangle)/2\} \otimes \{|H\rangle, |V\rangle, (|H\rangle - i|V\rangle)/2, (|H\rangle + |V\rangle)/2\}$ are needed. The 16 measurements can also be realized via a BD, two QWPs, three HWPs, and a PBS by setting the angles of the wave plates in different angles. The classical mutual information $I(AB:M) = H(\rho_{AB}) + H(\rho_M) - H(\rho_{ABM})$ with $H(\rho) = \sum_i -p_i\log_2 p_i$ can be obtained by projecting the state to the computational basis of both the qubits and the meter.

APPENDIX B: GENERALIZATION TO AN N-QUBIT CHAIN

The fueling mechanism can be extended to an N-qubit chain, where the low energy of the first qubit A can be upconverted to an arbitrary high energy of the last qubit B. The demonstration is illustrated in Fig. 5(a). At time $t = 0$, qubit A is excited, and the other qubits are initialized in the ground states. Subsequently, the coefficient g between qubit A and the second qubit is switched on with the Rabi frequency $\Omega_N = \sqrt{g^2 + \delta^2/(N-1)^2}$. At time $t = \pi/\Omega_N$, the energy of qubit A is measured. If it is found in the ground state, the excitation is successfully converted to the second qubit. Note that the process is equivalent to a measurement on the second qubit as two qubits are entangled and projective measurement on either qubit leads the other qubit to be in a maximal mixed state. The same task is applied between the excited second qubit and the third qubit. Repeating this process, finally the last qubit B can be excited with certain probability.

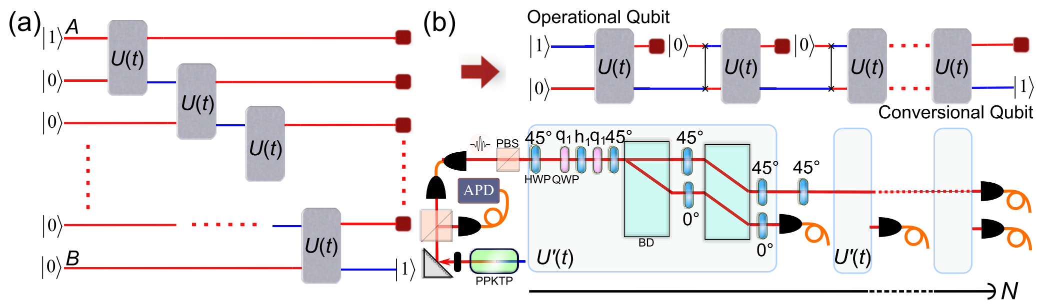

FIG. 5. Energy upconversion. (a) Circuit to achieve the energy upconversion in an N-qubit chain. (b) Upper panel: the simplified circuit of (a), which is achieved by translating measurements on different qubits into those on only two qubits at different times. Lower panel: experiment setup. By initializing the state of photons in $|LH\rangle$, the interaction is simply realized by two BDs and wave plates.

Through the qubit-efficient scheme [37], the quantum circuit in Fig. 5(a) can be further simplified to the one with two qubits, which are dubbed as the operational and conversional qubits. This is achieved by translating measurements on different qubits into those on only two qubits at different times. As shown in the upper panel in Fig. 5(b), we first initialize the state of the qubits to $|10\rangle$, and successively apply the unitary operator $U(t)$. A local projective measurement $|0\rangle\langle 0|$ is subsequently performed on the operational qubit. Before the output state is fed into the next interaction, a swap gate is applied to reset the state of the qubits to $|10\rangle$. The last local measurement on the operational qubit yields the conversional qubit being excited with probability $P_{\text{succ}} = \sin^{2(N-1)}\theta_N$.

The operational qubit is encoded in the spatial modes of the signal photons, i.e., $|L\rangle = |0\rangle$ and $|R\rangle = |1\rangle$, while the conversional qubit is encoded in the polarization states of the photons, $|H\rangle = |0\rangle$ and $|V\rangle = |1\rangle$. For interaction, the evolved two-qubit states $|\psi(t)\rangle = U(t)|RH\rangle$ can be rewritten as $|\psi(t)\rangle = U'(t)|LH\rangle$. Thus, the process of the interaction can be simulated by applying $U'(t)$ on the state of $|LH\rangle$. Similar to $U(t)$, the unitary operator $U'(t)$ can be decomposed as $U'(t) = \mathbb{L}\mathbb{T}\mathbb{M}'(t)\mathbb{R}'$ with $\mathbb{R}' = |L\rangle\langle L| \otimes (|H\rangle\langle V| + |V\rangle\langle H|) + |R\rangle\langle R| \otimes \mathbb{1}$ and $\mathbb{M}'(t) = |L\rangle\langle L| \otimes U_L(t) + |R\rangle\langle R| \otimes \mathbb{1}$. As illustrated in the lower panel of Fig. 5(b), the initial state $|LH\rangle$ is prepared by passing the heralded single photons through a PBS. The controlled transformations $\mathbb{R}'$ and $\mathbb{M}'(t)$ can be realized by inserting wave plates in the left mode of the photons, while $\mathbb{T}$ and $\mathbb{L}$ can be implemented by two BDs and HWPs with certain setting angles.

The local measurement is performed on the operational qubit by transmitting the photons in the left mode to the next step. By using a HWP setting at 45°, the photons are reset to the state of $|LH\rangle$ to feed into the second interaction. After $N-1$ times interaction and measurement, the successful probability of energy upconversion is the probability of the photons being found in the state of $|LV\rangle$.

[1] F. Jülicher, A. Ajdari, and J. Prost, Modeling molecular motors, Rev. Mod. Phys. **69**, 1269 (1997).

[2] G. Benenti, G. Casati, K. Saito, and R. S. Whitney, Fundamental aspects of steady-state conversion of heat to work at the nanoscale, Phys. Rep. **694**, 1 (2017).

[3] J. P. S. Peterson, R. S. Sarthour, and R. Laflamme, Implementation of a quantum engine fuelled by information, arXiv:2006.10136.

[4] H. E. D. Scovil and E. O. Schulz-DuBois, Three-Level Masers as Heat Engines, Phys. Rev. Lett. **2**, 262 (1959).

[5] V. Cimini, S. Gherardini, M. Barbieri, I. Gianani, M. Sbroscia, L. Buffoni, M. Paternostro, and F. Caruso, Experimental characterization of the energetics of quantum logic gates, npj Quantum Inf. **6**, 96 (2020).

[6] P. H. Souto Ribeiro, T. Häffner, G. L. Zanin, N. Rubiano da Silva, R. Medeiros de Araújo, W. C. Soares, R. J. de Assis, L. C. Céleri, and A. Forbes, Experimental study of the generalized Jarzynski fluctuation relation using entangled photons, Phys. Rev. A **101**, 052113 (2020).

[7] M. O. Scully, M. S. Zubairy, G. S. Agarwal, and H. Walther, Extracting work from a single heat bath via vanishing quantum coherence, Science **299**, 862 (2003).

[8] H. T. Quan, P. Zhang, and C. P. Sun, Quantum heat engine with multilevel quantum systems, Phys. Rev. E **72**, 056110 (2005).

[9] J.-S. Xu, M.-H. Yung, X.-Y. Xu, S. Boixo, Z.-W. Zhou, C.-F. Li, A. Aspuru-Guzik, and G.-C. Guo, Demon-like algorithmic quantum cooling and its realization with quantum optics, Nat. Photonics **8**, 113 (2014).

[10] Q. Bouton, J. Nettersheim, S. Burgardt, D. Adam, E. Lutz, and A. Widera, A quantum heat engine driven by atomic collisions, Nat. Commun. **12**, 2063 (2021).

[11] R. J. de Assis, T. M. de Mendonça, C. J. Villas-Boas, A. M. de Souza, R. S. Sarthour, I. S. Oliveira, and N. G. de Almeida, Efficiency of a Quantum Otto Heat Engine Operating under a Reservoir at Effective Negative Temperatures, Phys. Rev. Lett. **122**, 240602 (2019).

[12] W. Niedenzu, V. Mukherjee, A. Ghosh, A. G. Kofman, and G. Kurizki, Quantum engine efficiency bound beyond the second law of thermodynamics, Nat. Commun. **9**, 165 (2018).

[13] J. Roßnagel, O. Abah, F. Schmidt-Kaler, K. Singer, and E. Lutz, Nanoscale Heat Engine Beyond the Carnot Limit, Phys. Rev. Lett. **112**, 030602 (2014).

[14] J. P. Pekola, Towards quantum thermodynamics in electronic circuits, Nat. Phys. **11**, 118 (2015).

[15] J. Klatzow, J. N. Becker, P. M. Ledingham, C. Weinzetl, K. T. Kaczmarek, D. J. Saunders, J. Nunn, I. A. Walmsley, R. Uzdin, and E. Poem, Experimental Demonstration of Quantum Effects

in the Operation of Microscopic Heat Engines, Phys. Rev. Lett. **122**, 110601 (2019).
[16] V. Blickle and C. Bechinger, Realization of a micrometre-sized stochastic heat engine, Nat. Phys. **8**, 143 (2012).
[17] J. Roßnagel, S. T. Dawkins, K. N. Tolazzi, O. Abah, E. Lutz, F. Schmidt-Kaler, and K. Singer, A single-atom heat engine, Science **352**, 325 (2016).
[18] P. Strasberg, C. W. Wächtler, and G. Schaller, Autonomous Implementation of Thermodynamic Cycles at the Nanoscale, Phys. Rev. Lett. **126**, 180605 (2021).
[19] L. Buffoni, A. Solfanelli, P. Verrucchi, A. Cuccoli, and M. Campisi, Quantum Measurement Cooling, Phys. Rev. Lett. **122**, 070603 (2019).
[20] G. Manzano, F. Plastina, and R. Zambrini, Optimal Work Extraction and Thermodynamics of Quantum Measurements and Correlations, Phys. Rev. Lett. **121**, 120602 (2018).
[21] C. Elouard and A. N. Jordan, Efficient Quantum Measurement Engines, Phys. Rev. Lett. **120**, 260601 (2018).
[22] S. Seah, S. Nimmrichter, and V. Scarani, Maxwell's Lesser Demon: A Quantum Engine Driven by Pointer Measurements, Phys. Rev. Lett. **124**, 100603 (2020).
[23] S. K. Manikandan, C. Elouard, K. W. Murch, A. Auffèves, and A. N. Jordan, Efficiently fuelling a quantum engine with incompatible measurements, Phys. Rev. E **105**, 044137 (2022).
[24] J. Yi, P. Talkner, and Y. W. Kim, Single-temperature quantum engine without feedback control, Phys. Rev. E **96**, 022108 (2017).
[25] H. T. Quan, Y. D. Wang, Y.-X. Liu, C. P. Sun, and F. Nori, Maxwell's Demon Assisted Thermodynamic Cycle in Superconducting Quantum Circuits, Phys. Rev. Lett. **97**, 180402 (2006).
[26] C. Elouard, D. Herrera-Martí, B. Huard, and A. Auffèves, Extracting Work from Quantum Measurement in Maxwell's Demon Engines, Phys. Rev. Lett. **118**, 260603 (2017).
[27] P. Kammerlander and J. Anders, Coherence and measurement in quantum thermodynamics, Sci. Rep. **6**, 22174 (2016).
[28] K. Brandner, M. Bauer, M. T. Schmid, and U. Seifert, Coherence-enhanced efficiency of feedback-driven quantum engines, New J. Phys. **17**, 065006 (2015).
[29] J. P. Pekola, D. S. Golubev, and D. V. Averin, Maxwell's demon based on a single qubit, Phys. Rev. B **93**, 024501 (2016).
[30] H. Tajima and K. Funo, Superconducting-like Heat Current: Effective Cancellation of Current-Dissipation Trade-Off by Quantum Coherence, Phys. Rev. Lett. **127**, 190604 (2021).
[31] L. Bresque, P. A. Camati, S. Rogers, K. Murch, A. N. Jordan, and A. Auffèves, Two-Qubit Engine Fueled by Entanglement and Local Measurements, Phys. Rev. Lett. **126**, 120605 (2021).
[32] K. Wang, Y. Shi, L. Xiao, J. Wang, Y. N. Joglekar, and P. Xue, Experimental realization of continuous-time quantum walks on directed graphs and their application in PageRank, Optica **7**, 1524 (2020).
[33] K. Wang, X. Wang, X. Zhan, Z. Bian, J. Li, B. C. Sanders, and P. Xue, Entanglement-enhanced quantum metrology in a noisy environment, Phys. Rev. A **97**, 042112 (2018).
[34] R. Landauer, Irreversibility and heat generation in the computing process, IBM J. Res. Dev. **5**, 183 (1961).
[35] J. M. R. Parrondo, J. M. Horowitz, and T. Sagawa, Thermodynamics of information, Nat. Phys. **11**, 131 (2015).
[36] Y. Masuyama, K. Funo, Y. Murashita, A. Noguchi, S. Kono, Y. Tabuchi, R. Yamazaki, M. Ueda, and Y. Nakamura, Information-to-work conversion by Maxwell's demon in a superconducting circuit quantum electrodynamical system, Nat. Commun. **9**, 1291 (2018).
[37] K. Wang, L. Xiao, W. Yi, S.-J. Ran, and P. Xue, Experimental realization of a quantum image classifier via tensor-network-based machine learning, Photon. Res. **9**, 2332 (2021).
[38] L. Szilard, über die Entropieverminderung in einem thermodynamischen System bei Eingriffen intelligenter Wesen, Z. Phys. **53**, 840 (1929).
[39] S. W. Kim, T. Sagawa, S. De Liberato, and M. Ueda, Quantum Szilard Engine, Phys. Rev. Lett. **106**, 070401 (2011).
[40] J. P. S. Peterson, T. B. Batalhão, M. Herrera, A. M. Souza, R. S. Sarthour, I. S. Oliveira, and R. M. Serra, Experimental Characterization of a Spin Quantum Heat Engine, Phys. Rev. Lett. **123**, 240601 (2019).
[41] N. Cottet, S. Jezouin, L. Bretheau, P. Campagne-Ibarcq, Q. Ficheux, J. Anders, A. Auffèves, R. Azouit, P. Rouchon, and B. Huard, Observing a quantum Maxwell demon at work, Proc. Natl. Acad. Sci. U.S.A. **114**, 7561 (2017).
[42] M. Josefsson, A. Svilans, A. M. Burke, E. A. Hoffmann, S. Fahlvik, C. Thelander, M. Leijnse, and H. Linke, A quantum-dot heat engine operating close to the thermodynamic efficiency limits, Nat. Nanotechnol. **13**, 920 (2018).